The A dependence of the nuclear structure function ratios.

Arneodo, M.; Ballintijn, M.; van der Heijden, M.; de Jong, M.; Ketel, T.J.; van Middelkoop, G.

published in
Nuclear Physics B
1996

DOI (link to publisher)
10.1016/S0550-3213(96)00536-6

document version
Publisher's PDF, also known as Version of record

ELSEVIER

Nuclear Physics B 481 (1996) 3–22

NUCLEAR PHYSICS B

The A dependence of the nuclear structure function ratios

The New Muon Collaboration (NMC)

M. Arneodo[ℓ,1], A. Arvidson[m], B. Badełek[m,o], M. Ballintijn[h], G. Baum[a], J. Beaufays[h], I.G. Bird[c,h,2], P. Björkholm[m], M. Botje[k,3], C. Broggini[g,4], W. Brückner[c], A. Brüll[b,5], W.J. Burger[k,6], J. Ciborowski[o], R. van Dantzig[h], A. Dyring[m], H. Engelien[b], M.I. Ferrero[ℓ], L. Fluri[g], U. Gaul[c], T. Granier[i,7], M. Grosse-Perdekamp[b,8], D. von Harrach[c,9], M. van der Heijden[h], C. Heusch[j], Q. Ingram[k], M. de Jong[h,2], E.M. Kabuß[c,9], R. Kaiser[b], T.J. Ketel[h], F. Klein[e,10], S. Kullander[m], K. Kurek[o], U. Landgraf[b], T. Lindqvist[m], G.K. Mallot[e], C. Mariotti[ℓ,11], G. van Middelkoop[h], A. Milsztajn[i], Y. Mizuno[c,12], A. Most[c,13], A. Mücklich[c], J. Nassalski[n], D. Nowotny[c], J. Oberski[h], A. Paić[g], C. Peroni[ℓ], B. Povh[c,d], K. Prytz[m,14], R. Rieger[e], K. Rith[c,15], K. Röhrich[e,16], E. Rondio[n,2], L. Ropelewski[o,2], A. Sandacz[n], D. Sanders[17], C. Scholz[c], R. Seitz[e,18], F. Sever[a,h,19], T.-A. Shibata[d,20], M. Siebler[a], A. Simon[c,21], A. Staiano[ℓ], M. Szleper[n], W. Tłaczała[n,22] Y. Tzamouranis[c,17], M. Virchaux[i], J.L. Vuilleumier[g], T. Walcher[e], R. Windmolders[f], A. Witzmann[b], K. Zaremba[n,22] F. Zetsche[c,23]

[a] *Bielefeld University, Bielefeld, Germany*[24]
[b] *Freiburg University, Freiburg, Germany*[24]
[c] *Max-Planck Institut für Kernphysik, Heidelberg, Germany*[24]
[d] *Heidelberg University, Heidelberg, Germany*[24]
[e] *Mainz University, Mainz, Germany*[24]
[f] *Mons University, Mons, Belgium*
[g] *Neuchâtel University, Neuchâtel, Switzerland*
[h] *NIKHEF, Amsterdam, The Netherlands*[25]
[i] *Saclay DAPNIA/SPP, Saclay, France*[27]
[j] *University of California, Santa Cruz, USA*

PII S0550-3213(96)00536-6

[k] Paul Scherrer Institut, Villigen, Switzerland
[f] Torino University and INFN Torino, Turin, Italy
[m] Uppsala University, Uppsala, Sweden
[n] Soltan Institute for Nuclear Studies, Warsaw, Poland[26]
[o] Warsaw University, Warsaw, Poland[26]

Received 3 September 1996; accepted 23 September 1996

Abstract

Results are presented for six nuclei from Be to Pb on the structure function ratios $F_2^A/F_2^C(x)$ and their A dependence in deep inelastic muon scattering at 200 GeV incident muon energy. The data cover the kinematic range $0.01 < x < 0.8$ with Q^2 ranging from 2 to 70 GeV^2. The A dependence of nuclear structure function ratios is parametrised and compared to various models.

1. Introduction

The structure function F_2 for a bound nucleon, measured in deep inelastic scattering (DIS) of leptons, differs from that for a free nucleon. Such nuclear effects have been actively investigated over the past decade [1]. The data are usually presented in terms

[1] Alexander von Humboldt fellow.
[2] Now at CERN, 1211 Genève 23, Switzerland.
[3] Now at NIKHEF, 1009 DB Amsterdam, The Netherlands.
[4] Now at University of Padova, 35131 Padova, Italy.
[5] Now at MPI für Kernphysik, 69029 Heidelberg, Germany.
[6] Now at Université de Genève, 1211 Genève 4, Switzerland.
[7] Now at DPTA, CEA, Bruyères-le-Chatel, France.
[8] Now at Yale University, New Haven, 06511 CT, USA.
[9] Now at University of Mainz, 55099 Mainz, Germany.
[10] Now at University of Bonn, 53115 Bonn, Germany.
[11] Now at INFN-Istituto Superiore di Sanità, 00161 Roma, Italy.
[12] Now at Osaka University, 567 Osaka, Japan.
[13] Now at University of Michigan, Michigan, USA.
[14] Now at Stockholm University, 113 85 Stockholm, Sweden.
[15] Now at University of Erlangen-Nürnburg, 91058 Erlangen, Germany.
[16] Now at IKP2-KFA, 52428 Jülich, Germany.
[17] Now at University of Houston, 77204 TX, USA.
[18] Now at Dresden University, 01062 Dresden, Germany.
[19] Now at ESRF, 38043 Grenoble, France.
[20] Now at Tokyo Institute of Technology, Japan.
[21] Now at University of Freiburg, 79104 Freiburg, Germany.
[22] Now at Warsaw University of Technology, Warsaw, Poland.
[23] Now at DESY, 22603 Hamburg, Germany.
[24] Supported by Bundesministerium für Bildung und Forschung.
[25] Supported in part by FOM, Vrije Universiteit Amsterdam and NWO.
[26] Supported by KBN SPUB Nr 621/E - 78/SPUB/P3/209/94.
[27] Laboratory of CEA, Direction des Sciences de la Matière.

of the ratio F_2^A/F_2^D, where F_2^A and F_2^D are structure functions per nucleon of nucleus A and the deuteron, respectively. Since the nucleons in the deuteron are only weakly bound, F_2^D is a good approximation for the structure function of a free nucleon.

For values of the Bjorken scaling variable $x \lesssim 0.05$, the ratio F_2^A/F_2^D is smaller than unity, a fact known as "shadowing". In the intermediate x range, $0.05 \lesssim x \lesssim 0.2$, the ratio shows a small enhancement over unity. For larger values of x, up to about 0.6, the ratio decreases with increasing x. The size of all these effects increases with the atomic number A. In the kinematic range explored so far there is little or no evidence for a dependence on the photon virtuality Q^2.

Attempts have been made to describe shadowing in terms of generalised vector meson dominance or of parton–parton fusion. At larger values of x the observed phenomena have been discussed within "conventional nuclear physics" models, describing the effect of the nuclear potential on the bound nucleons by means of a reduced effective nucleon mass, often accompanied by an increased density of virtual pions. Alternatively, an increase of the quark confinement size in the nucleus has been invoked. In spite of the variety of theoretical approaches proposed, a quantitative understanding of the basic mechanisms responsible for the observed effects is still lacking.

While the A dependence of nuclear effects in structure functions has been studied in detail at large x [1], in the small x region accurate data are available only for a few light nuclei [2,3]. In this paper we present a study of nuclear effects for a wide range of A, in the kinematic region $0.01 < x < 0.8$ and $2 < Q^2 < 70$ GeV^2. For the present data, carbon – and not the deuteron – was chosen as the reference nucleus; the results will thus be given in the form F_2^A/F_2^C. The choice of carbon was motivated by the requirement of large target thicknesses. The other target materials were Be, Al, Ca, Fe, Sn and Pb. The present results, in conjunction with earlier ones on D, He, Li, C and Ca [2,3], allow a detailed investigation of the A dependence of the bound nucleon structure function in the shadowing and enhancement regions.

In deep inelastic muon scattering from a nucleon, the double differential cross section per nucleon for one-photon exchange is given by

$$\frac{d^2\sigma_{1\gamma}}{dx\,dQ^2} = \frac{4\pi\alpha^2}{Q^4}\frac{F_2(x,Q^2)}{x}\left[1 - y - \frac{Q^2}{4E^2} + \left(1 - \frac{2m_\mu^2}{Q^2}\right)\frac{y^2 + Q^2/E^2}{2[1 + R(x,Q^2)]}\right], \quad (1)$$

where $F_2(x,Q^2)$ is the structure function of the nucleon and $R(x,Q^2)$ is the ratio of the longitudinally to transversely polarised virtual photon absorption cross sections. The variable $-Q^2$ is the four-momentum of the virtual photon squared, E the incident muon energy, α the electromagnetic coupling constant and m_μ the muon mass. The Bjorken scaling variable x, and y are defined as $x = Q^2/2M\nu$ and $y = \nu/E$, where ν is the energy of the virtual photon in the laboratory frame and M the proton mass. The function $R(x,Q^2)$ is taken to be independent of the nuclear mass A, an assumption supported by experimental data for $x > 0.0085$ and $Q^2 > 2$ GeV^2 [4,5]. Under this assumption the structure function ratio F_2^A/F_2^C becomes equal to the corresponding cross section ratio.

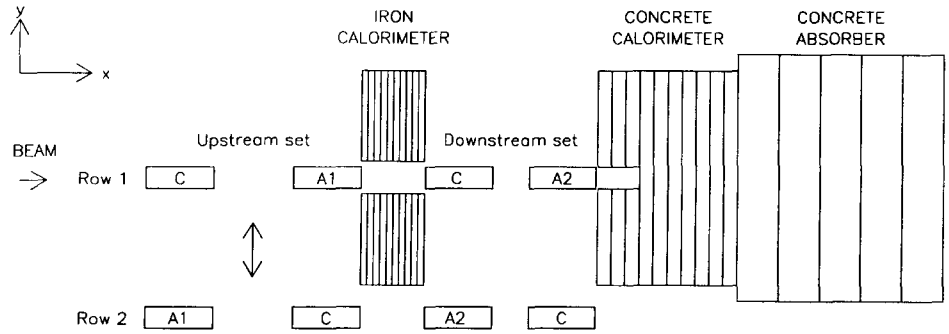

Fig. 1. Target calorimeters and complementary target set-up. The total dimensions are 8 m and 2.4 m along the x and y directions, respectively.

The paper is organised as follows. In Section 2 the features of the experiment relevant to the present analysis are described, in Section 3 the analysis is discussed and the results are presented in Section 4.

2. The experimental set-up

The experiment was performed with the NMC spectrometer at the CERN SPS muon beam line M2. The incident muon energy was 200 GeV. A detailed description of the spectrometer can be found in Ref. [6]. In the following we only give a description of the target set-up and of the trigger conditions.

To perform accurate measurements of cross section ratios, a complementary target set-up was used; similar set-ups were employed in other NMC experiments. Two target sets were used, an upstream and a downstream one (Fig. 1). Each set consisted of two pairs of targets which were alternately exposed to the beam. One pair contained a target of material A1 and a carbon target, one behind the other along the beam direction; in the second, complementary pair, the positions of the two targets were interchanged. The pairs of targets were alternately placed in the beam, for about 40 minutes each. Each target in a pair received the same muon flux. Furthermore, the geometrical detector acceptance for events with a vertex at a given position along the beam was independent of the target material. The second set of targets consisted of a similar arrangement of two pairs of targets, placed further down the beam line; in this set material A2 was not necessarily the same as material A1 of the first set. As a pair of targets from each set was placed in the beam at the same time, two ratios of cross sections, A1/C and A2/C, were determined simultaneously in two semi-independent measurements. With these complementary target arrangements, the cross section ratio, σ^{A}/σ^{C}, for nucleus A and carbon can be expressed in a way that depends only on the number of reconstructed events, N, and on the number of nucleons per unit area, T, in the target [6]:

$$\left(\frac{\sigma^{A}}{\sigma^{C}}\right)_{meas} = \sqrt{\left(\frac{N^{A}_{Row1} \cdot N^{A}_{Row2}}{N^{C}_{Row1} \cdot N^{C}_{Row2}}\right) \cdot \left(\frac{T^{C}_{Row1} \cdot T^{C}_{Row2}}{T^{A}_{Row1} \cdot T^{A}_{Row2}}\right)}. \quad (2)$$

In this way geometrical acceptance and detector efficiencies cancel, as do the beam fluxes. The formula was applied separately to the upstream and downstream target sets. The frequent exchange of the target rows substantially eliminated the effects of possible time dependence of the acceptance and efficiency of the apparatus.

Table 1
Target configurations (see text)

Row	I	II	III	IV	V	VI	VII
1	C Al C Pb	C Pb C Al	C Fe C Fe	C Pb C Pb	C Be C Ca	C Ca C Be	C Sn C Sn
2	Al C Pb C	Pb C Al C	Fe C Fe C	Pb C Pb C	Be C Ca C	Ca C Be C	Sn C Sn C

Table 2
Parameters characterising the targets used in the measurements. The nuclear densities were calculated as $3A/4\pi R_e^3$ with $R_e^2 = 5\langle r^2\rangle/3$ and $\langle r^2\rangle$, the mean square charge radii of the nuclei, which were taken from Ref. [17]

Target	A	Density	Thickness			Nucl. dens.
		[g/cm^2]	[X_0]	[λ_I]	[g/cm^2]	[nucl./fm^3]
Beryllium	9.01	1.85	2.13	1.84	138.8	0.063
Carbon	12.01	1.90	3.99	1.65	143.1	0.088
Aluminium	26.98	2.72	5.66	1.28	135.9	0.106
Calcium	40.08	1.55	7.21	3.09	115.6	0.106
Iron	55.85	7.83	9.90	1.04	137.0	0.117
Tin	118.69	7.31	16.67	0.92	149.3	0.130
Lead	207.19	11.27	15.51	0.51	98.8	0.138

The data were collected with seven target configurations, listed in Table 1. The data for each of the target configurations I to VI were collected during a few days in 1989; the data for configuration VII were taken in a one month long period in 1988. The targets had a similar number of nucleons/cm^2, providing optimal statistical accuracy for the cross section ratio measurement. The parameters characterising the targets are given in Table 2. The Be, C and Ca targets consisted of 75 cm long cylinders; the Al, Fe, Sn and Pb targets of several equally spaced slices distributed over a length of 75 cm. The diameter of the targets was 7.5 cm. All targets were of natural isotopic composition.

The total target thickness exposed to the beam was 500–600 g/cm^2. The spectrometer was shielded from electromagnetic and hadronic background originating in such an amount of material by a calorimetric set-up [7] (see Fig. 1), consisting of an iron-scintillator trigger calorimeter, a concrete-scintillator trigger calorimeter and a concrete absorber. The iron calorimeter was located between the upstream and downstream target sets; the concrete calorimeter was installed downstream of the targets. This arrangement

made it possible to detect all hadronic showers emerging with angles of up to 20° with respect to the beam direction. In this way, for all events in which the scattered muon was seen by the NMC spectrometer, the accompanying hadrons were also measured. Thus the iron and concrete calorimeters tagged deep inelastic interactions by the detection of the hadronic showers. The energy resolution for pions was about 25% at 10 GeV and 16% at 100 GeV. The calorimeter information was used only at the trigger level.

The choice of iron for the upstream calorimeter was motivated by the small space available between the targets. Concrete was preferred for the downstream calorimeter and for the absorber so as to minimise the multiple scattering of the outgoing muon. For the same reason, the iron calorimeter had a rectangular hole around the beam axis, with a size matching the geometrical acceptance of the forward spectrometer magnet (FSM) used to measure the scattered muon momentum. Forward hadrons passing through this hole were detected in the concrete calorimeter.

The iron and concrete calorimeters each consisted of ten layers of active (scintillator) and passive (iron or concrete) material. The active area was 1.8×1.8 m^2. The iron (concrete) calorimeter had a total depth of 0.65 m (1.15 m), corresponding to 23 (8.6) radiation lengths, X_0, or 2.4 (2.3) nuclear interaction lengths, λ_I. In order to resolve events originating from the most downstream target, the concrete calorimeter had an 8 cm wide and 33 cm deep hole (see Fig. 1). The depth of the absorber was 1.82 m ($17.1X_0$, $4.6\lambda_I$), sufficient to contain all showers from the calorimeters; its area covered the FSM aperture.

An energy deposit in the calorimeter above a given threshold was required for an event to be triggered. Muon interactions in the absorber did not release energy in the calorimeters and were therefore suppressed. A threshold corresponding to an energy release of 4 GeV for a hadronic shower gave a trigger efficiency close to 100%. In addition to the requirement of an energy deposit in the calorimeter, the standard "T1" trigger conditions described in Ref. [6] were applied, essentially demanding that a scattered muon be detected. The trigger was sensitive to muons scattered by more than 1° with respect to the incoming beam direction.

3. Analysis

Various kinematic cuts were applied to the data. Events from regions with rapidly changing acceptance (scattering angle $\vartheta < 13$ mrad) and poor spectrometer resolution ($\nu < 17$ GeV) were removed. The requirement $y < 0.85$ excluded kinematic regions where radiative corrections are large. The condition $p' > 30$ GeV was imposed on the scattered muon momentum, thereby rejecting muons originating from hadron decays. Events with poor vertex resolution due to multiple scattering, which is proportional to $1/(p'\vartheta)$, were suppressed by applying the cut $x > 0.01$, which corresponds to $p'\vartheta \gtrsim 1000$ GeV· mrad. The numbers of remaining events are 0.4×10^6 for Be/C, Ca/C, Al/C and Fe/C, 0.6×10^6 for Pb/C, and 2.8×10^6 for Sn/C. These data cover the kinematic region $0.01 < x < 0.8$ and $2 < Q^2 < 70$ GeV^2.

In order to obtain the one-photon exchange cross section ratio $(\sigma^A/\sigma^C)_{1\gamma}$ from the measured cross section ratio (Eq. (2)), the measured yields were corrected for higher order electroweak processes, notably for the radiative tails of coherent scattering from nuclei and quasielastic scattering from nucleons, as well as for the inelastic radiative tail. The threshold of the target calorimeter was equivalent to the energy release of 40–45 minimum ionising particles, which corresponded to 4 GeV for hadronic showers, as mentioned earlier, and to a somewhat lower energy for electromagnetic ones. For coherent and quasielastic events the ν cut of 17 GeV requires a minimum energy of the radiated photon of about 10 GeV. This means that also these events satisfied the trigger condition, thereby requiring the application of the full coherent and quasielastic radiative corrections.

Each event was weighted with the correction factor $\eta = \sigma_{1\gamma}/\sigma_{\text{meas}}$, which was computed according to the scheme of Akhundov et al. [8]. Multiphoton exchange processes in the coherent radiative tail were also taken into account [9]; they were relevant only for the Sn and Pb targets, for which they amounted to less than 3% of the total radiative correction in the small x region.

The calculation of the quasielastic radiative tails requires a parametrisation of the nucleon form factor which was taken from Ref. [10]. The quasielastic suppression factor, which takes into account the reduction of the elastic cross section of the bound nucleon with respect to the free one, was evaluated using the results of Bernabeu [11] for carbon and of Moniz [12] for the other nuclei. For the evaluation of the coherent radiative tails, the nuclear elastic form factors are needed. A parametrisation of the electric and magnetic form factors for ^{9}Be was taken from Ref. [13]. The form factors of the other nuclei were calculated using the Fourier transform of their charge distributions. These were determined in terms of sums of Gaussians for ^{12}C [14], ^{40}Ca [15] and ^{208}Pb [16], by a Fourier–Bessel analysis for ^{27}Al and ^{56}Fe [17] and in the framework of a three-parameter Gaussian model for ^{117}Sn [18].

Finally, in order to determine the inelastic tail contribution, the knowledge of $R(x,Q^2)$ and $F_2^A(x,Q^2)$ is needed. The ratio $R(x,Q^2)$ was taken from the SLAC parametrisation [19] and was assumed to be independent of the atomic mass A. The structure functions $F_2^C(x,Q^2)$ and $F_2^A(x,Q^2)$ were obtained using a parametrisation of F_2^D [20], the ratio F_2^C/F_2^D [2] and the presently measured ratio F_2^A/F_2^C:

$$F_2^C(x,Q^2) = F_2^D(x,Q^2)\frac{F_2^C}{F_2^D}(x), \qquad F_2^A(x,Q^2) = F_2^C(x,Q^2)\frac{F_2^A}{F_2^C}(x), \tag{3}$$

where the cross section ratios were assumed to be independent of Q^2. For the ratio F_2^A/F_2^C, the presently measured cross section ratios as well as those from the E139 experiment [21] were used. Since the measured ratio is needed as an input, an iterative procedure was required.

The radiative correction factors, η, for the individual targets may vary over a wide range; in the case of lead from 0.3 at small x to 1.2 at large x. The dominant contribution to η stems from the coherent radiative tail. For the ratios however, the largest resulting total corrections are 0.85 for C/Be, 0.8 for Al/C, 0.6 for Ca/C and for Fe/C and 0.4

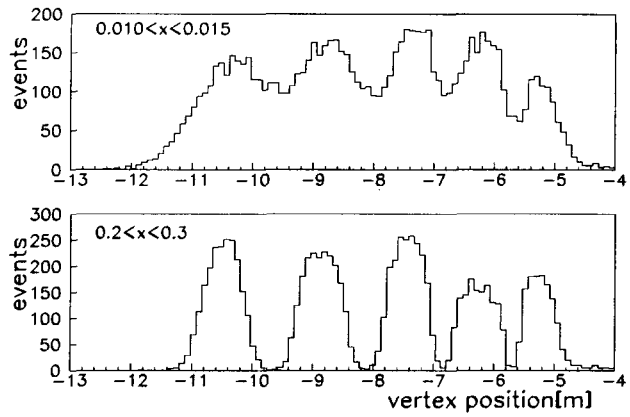

Fig. 2. The vertex distribution along the beam direction for two x bins – the lowest bin (top) and an intermediate one (bottom). The events originate (left to right) from a carbon, an aluminium, a carbon and a lead target, respectively. The events around vertex position -5 m come from the concrete calorimeter. The vertex position is measured from the center of the FSM.

for Sn/C and for Pb/C in the lowest x bin. Their size decreases rapidly with increasing x and differs from unity by less than 0.01 for $x > 0.06$.

The data were also corrected for the non-isoscalarity of the targets using a parametrisation of the structure function ratio F_2^n/F_2^p [6]. This correction is maximum at large x where it is at most 15% for the ratio $F_2^{\mathrm{Pb}}/F_2^{\mathrm{C}}$; it is negligible at small x.

The finite resolution of the spectrometer leads to an uncertainty in the position of the interaction vertex and in the determination of the kinematic variables. The dominant source of this smearing is multiple scattering of the muon which strongly affects events with small $p'\vartheta$ (small x). In Fig. 2 the vertex distributions for the smallest and an intermediate x bin are shown. The effects of the smearing on the cross section ratios were estimated by a Monte Carlo simulation.

In the Monte Carlo simulation hits in the detectors were generated for the incident and scattered muon tracks according to parametrisations of the measured efficiencies of the tracking chambers and trigger hodoscopes. In order to take into account the multiple scattering and the energy loss of the muon, a detailed description of the geometry and composition of the targets and of the target calorimeters was used. The Monte Carlo events were passed through the same reconstruction programs as the data. Each event was weighted with the inclusive cross section, i.e. the one-photon exchange cross section together with contributions from radiative and other higher order processes.

The Monte Carlo simulation reproduces the data well for all target configurations. As an example, Fig. 3 shows the ratio of the data and Monte Carlo vertex distributions along the beam direction for the C,Al and C,Pb target configurations for the x bins shown in Fig. 2.

In Fig. 4, the factors to correct the ratio $F_2^{\mathrm{Fe}}/F_2^{\mathrm{C}}$ for the effects of smearing are shown. The correction to the ratio is small because the loss of events from a given target is compensated by the gain of events from the adjacent ones. For the smallest value of x

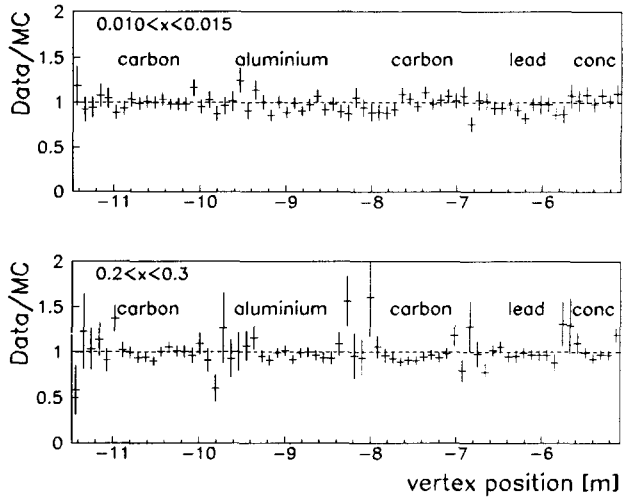

Fig. 3. Ratio of data and Monte Carlo yields as a function of the vertex position along the beam direction for two x bins for the same target configuration as shown in Fig. 2. The concrete calorimeter is indicated as "conc".

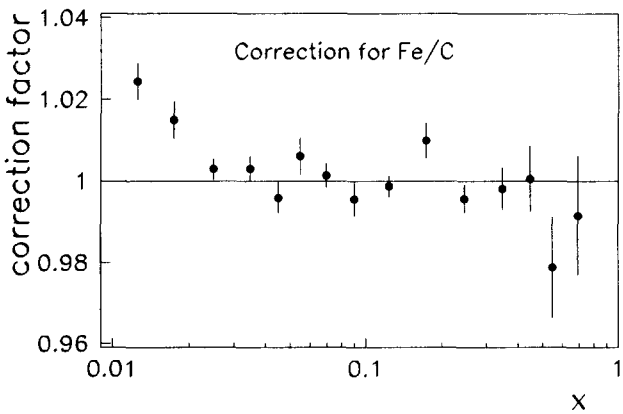

Fig. 4. The factors to correct the ratio F_2^{Fe}/F_2^C for the effects of smearing as a function of x. The errors shown are statistical.

the correction factor ranges from 1.02 for Be/C to 1.04 for Pb/C. Events originating in the detectors close to the target region lead to a correction of up to 0.5% for the ratios of the upstream target set.

As a check of the method used to calculate the cross section ratio, following the reasoning presented in Ref. [6], the ratio of the beam fluxes was evaluated from the measured number of events. This flux ratio was studied as a function of all measured kinematic variables and, after applying all corrections, was found to be independent of them in the range where the results are presented.

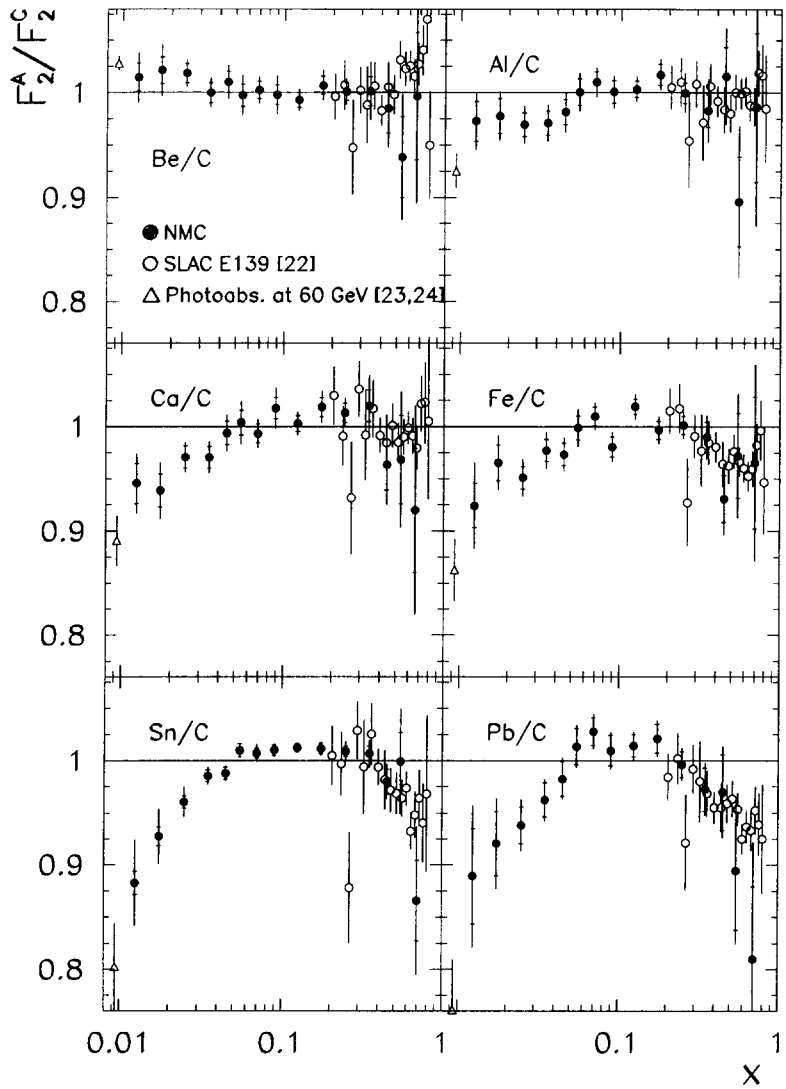

Fig. 5. Structure function ratios as a function of x, averaged over Q^2. The inner error bars represent the statistical uncertainty, the outer errors the statistical and systematic uncertainties added in quadrature. The E139 data for silver and gold were used for the comparison with our tin and lead data, respectively. The photo-absorption cross section data are plotted at $x \sim 0.01$.

4. The results

All cross section ratios measured with the same pair of target materials were found to agree and the data were therefore combined. The x dependences of the structure function ratios F_2^A/F_2^C, averaged over Q^2, are presented in Fig. 5 and in Tables 3–8. The mean Q^2 and mean y for each x bin are also given in the tables. The inner error bars in Fig. 5

Table 3
The ratio F_2^{Be}/F_2^C as a function of x. The x value, the mean Q^2 and the mean y are also given. The normalisation error on the ratio is 0.002 and is not included in the systematic uncertainty

x	$\langle Q^2 \rangle$ [GeV^2]	$\langle y \rangle$	$F_2^{Be}/F_2^C \pm$ stat. $\pm$ syst.
0.0125	3.4	0.73	1.014±0.013±0.020
0.0175	4.5	0.69	1.021±0.013±0.021
0.0250	6.0	0.66	1.019±0.009±0.009
0.0350	8.0	0.62	1.000±0.009±0.010
0.0450	9.8	0.59	1.010±0.010±0.013
0.0550	11.4	0.57	0.997±0.011±0.016
0.0700	13.8	0.54	1.002±0.008±0.010
0.0900	16.8	0.51	0.998±0.009±0.016
0.1250	21.4	0.47	0.993±0.007±0.008
0.1750	27.6	0.43	1.007±0.008±0.012
0.2500	35.5	0.39	1.001±0.008±0.010
0.3500	45.4	0.36	1.001±0.014±0.024
0.4500	53.9	0.33	0.985±0.023±0.029
0.5500	60.5	0.30	0.938±0.038±0.046
0.7000	66.7	0.26	0.997±0.061±0.082

Table 4
The ratio F_2^{Al}/F_2^C as a function of x. The x value, the mean Q^2 and the mean y are also given. The normalisation error on the ratio is 0.002 and is not included in the systematic uncertainty

x	$\langle Q^2 \rangle$ [GeV^2]	$\langle y \rangle$	$F_2^{Al}/F_2^C \pm$ stat. $\pm$ syst.
0.0125	3.4	0.73	0.973±0.019±0.020
0.0175	4.5	0.69	0.978±0.016±0.016
0.0250	6.1	0.66	0.969±0.011±0.014
0.0350	8.0	0.62	0.971±0.011±0.013
0.0450	9.8	0.59	0.981±0.012±0.015
0.0550	11.6	0.57	1.000±0.013±0.013
0.0700	13.9	0.54	1.010±0.010±0.010
0.0900	16.9	0.51	1.001±0.011±0.011
0.1250	21.3	0.47	1.003±0.008±0.009
0.1750	27.4	0.43	1.017±0.010±0.011
0.2500	35.5	0.39	0.999±0.010±0.016
0.3500	45.3	0.35	0.983±0.016±0.026
0.4500	52.9	0.32	1.016±0.028±0.036
0.5500	58.2	0.29	0.896±0.043±0.058
0.7000	63.9	0.25	0.986±0.071±0.089

represent the statistical uncertainties including those of the smearing correction factors. The outer error bars indicate the size of the statistical and systematic uncertainties added in quadrature.

In the present results the main contributions to the systematic errors at small x are the uncertainties of the radiative corrections. These uncertainties were estimated by varying the input parameters to the radiative correction program following the procedure outlined in Ref. [6].

Other contributions to the systematic error at small x include the uncertainty of the

Table 5
The ratio F_2^{Ca}/F_2^C as a function of x. The x value, the mean Q^2 and the mean y are also given. The normalisation error on the ratio is 0.003 and is not included in the systematic uncertainty

x	$\langle Q^2 \rangle$ [GeV^2]	$\langle y \rangle$	$F_2^{Ca}/F_2^C \pm$ stat. $\pm$ syst.
0.0125	3.4	0.73	0.945±0.019±0.021
0.0175	4.5	0.69	0.939±0.016±0.022
0.0250	6.0	0.66	0.971±0.011±0.010
0.0350	7.9	0.62	0.970±0.011±0.011
0.0450	9.7	0.59	0.994±0.011±0.013
0.0550	11.4	0.57	1.004±0.012±0.017
0.0700	13.8	0.54	0.994±0.009±0.010
0.0900	16.7	0.51	1.018±0.010±0.017
0.1250	21.2	0.47	1.003±0.007±0.008
0.1750	27.4	0.43	1.019±0.009±0.012
0.2500	35.3	0.39	1.013±0.009±0.011
0.3500	45.3	0.36	1.020±0.015±0.025
0.4500	53.6	0.33	0.964±0.024±0.030
0.5500	60.3	0.30	0.968±0.042±0.049
0.7000	66.4	0.26	0.920±0.059±0.081

Table 6
The ratio F_2^{Fe}/F_2^C as a function of x. The x value, the mean Q^2 and the mean y are also given. The normalisation error on the ratio is 0.002 and is not included in the systematic uncertainty

x	$\langle Q^2 \rangle$ [GeV^2]	$\langle y \rangle$	$F_2^{Fe}/F_2^C \pm$ stat. $\pm$ syst.
0.0125	3.4	0.73	0.924±0.021±0.036
0.0175	4.5	0.70	0.965±0.017±0.020
0.0250	6.1	0.66	0.951±0.011±0.014
0.0350	8.1	0.63	0.977±0.011±0.014
0.0450	10.0	0.60	0.973±0.011±0.013
0.0550	11.8	0.58	0.999±0.011±0.014
0.0700	14.1	0.55	1.010±0.009±0.010
0.0900	17.1	0.52	0.981±0.009±0.011
0.1250	21.7	0.48	1.019±0.007±0.009
0.1750	27.8	0.43	0.997±0.009±0.010
0.2500	35.7	0.39	1.001±0.009±0.010
0.3500	45.4	0.35	0.990±0.014±0.015
0.4500	53.6	0.32	0.931±0.022±0.026
0.5500	60.3	0.30	0.972±0.041±0.044
0.7000	66.6	0.26	0.965±0.063±0.069

smearing correction. This was estimated by changing the vertex resolution as obtained from the Monte Carlo simulation by up to 3%, hence effectively modifying the amount of multiple Coulomb scattering.

The target calorimeter efficiency was only measured for Sn and C [22,23] where its effect on the ratio was typically less than one per cent, except at large x where it reached about 2%. The other ratios were not corrected for the target calorimeter efficiency. A systematic error equal to the full correction for the Sn/C ratio was assumed.

The uncertainty of the measurement of incoming ($\delta p/p = 0.2\%$) and scattered muon

Table 7
The ratio F_2^{Sn}/F_2^C as a function of x. The x value, the mean Q^2 and the mean y are also given. The normalisation error on the ratio is 0.002 and is not included in the systematic uncertainty

x	$\langle Q^2 \rangle$ [GeV^2]	$\langle y \rangle$	$F_2^{Sn}/F_2^C \pm$ stat. $\pm$ syst.
0.0125	3.2	0.71	0.883±0.011±0.040
0.0175	4.3	0.68	0.927±0.009±0.025
0.0250	5.6	0.62	0.960±0.006±0.013
0.0350	7.3	0.56	0.985±0.006±0.006
0.0450	8.6	0.50	0.988±0.006±0.004
0.0550	9.8	0.45	1.010±0.006±0.002
0.0700	11.2	0.40	1.007±0.005±0.007
0.0900	12.7	0.33	1.010±0.005±0.003
0.1250	14.8	0.28	1.012±0.004±0.003
0.1750	17.3	0.20	1.012±0.005±0.004
0.2500	20.5	0.16	1.009±0.005±0.008
0.3500	25.1	0.15	1.007±0.007±0.011
0.4500	32.0	0.15	0.980±0.012±0.012
0.5500	43.9	0.16	0.999±0.028±0.042
0.7000	56.8	0.24	0.866±0.038±0.060

Table 8
The ratio F_2^{Pb}/F_2^C as a function of x. The x value, the mean Q^2 and the mean y are also given. The normalisation error on the ratio is 0.002 and is not included in the systematic uncertainty

x	$\langle Q^2 \rangle$ [GeV^2]	$\langle y \rangle$	$F_2^{Pb}/F_2^C \pm$ stat. $\pm$ syst.
0.0125	3.4	0.73	0.889±0.046±0.050
0.0175	4.5	0.69	0.921±0.031±0.030
0.0250	6.1	0.66	0.938±0.018±0.017
0.0350	8.0	0.62	0.962±0.016±0.012
0.0450	9.8	0.59	0.982±0.017±0.012
0.0550	11.6	0.57	1.014±0.017±0.011
0.0700	13.9	0.54	1.028±0.013±0.011
0.0900	16.9	0.51	1.010±0.014±0.010
0.1250	21.4	0.47	1.014±0.011±0.008
0.1750	27.5	0.43	1.021±0.013±0.010
0.2500	35.5	0.39	0.996±0.012±0.010
0.3500	45.3	0.35	0.973±0.021±0.015
0.4500	53.6	0.32	0.970±0.036±0.024
0.5500	60.0	0.30	0.894±0.057±0.041
0.7000	66.1	0.26	0.810±0.069±0.088

momenta ($\delta p'/p' = 0.2\%$) and the uncertainty introduced by the isoscalarity correction were also taken into account. They were relevant only at large x, where the former amounted to 0.1% for all ratios and the latter to 0.4% for the F_2^{Pb}/F_2^C ratio.

An additional systematic error was included as an estimate of the uncertainty of the method to extract the ratios (Eq. (2)). This error was evaluated as the difference between the present results and those determined as follows. The yield of the ith target in row j, N_{ij}, is given by $N_{ij} = \sum_{k=1}^{5} \sigma_{kj} T_{kj} \phi_j \epsilon_{kj} a_{ikj}$, where σ_{kj} is the total cross section of target material k, T_{kj} the thickness of target k, ϕ_j the muon flux, ϵ_{kj} the average

geometric acceptance of target k and a_{ikj} takes into account the smearing effects. The coefficients a_{ikj} were determined using the Monte Carlo simulation described above. A fit was performed in each x bin to the number of events from the eight targets and from the concrete calorimeter for each row. The fit parameters were the cross section ratios, σ^A/σ^C, the flux ratio for the two target rows, the ratios of the geometric acceptances for different target positions and a normalisation constant. The fitted structure function ratios were found to agree with those obtained using Eq. (2) to within 0.5% over most of the x range and 2% at small x.

The normalisation uncertainty on the ratios is due to the uncertainties in the target thicknesses and amounts to 0.2–0.3%, depending on the material. It is not included in the errors shown in Fig. 5.

At small x, the results for the structure function ratios are sensitive to the assumption $\Delta R^A \equiv R^A - R^C = 0$. The difference ΔR^A has been measured for Ca [5] and Sn [22]; the results are consistent with zero and have a total error of typically ± 0.04. If a value of $\Delta R^A = \pm 0.04$ is assumed, the ratios change by up to ∓ 0.01 at small x. This was not included in the systematic error.

All structure function ratios presented in Fig. 5 show a characteristic x dependence at small and intermediate x. There is a depletion below unity at small x, which increases with decreasing x. The ratio F_2^{Be}/F_2^C has the opposite behaviour since beryllium has a smaller A than carbon. The data show a clear and systematic increase of shadowing with increasing nuclear mass A.

Fig. 5 also shows the results for real ($Q^2 = 0$ GeV^2) photons of 60 GeV [24,25]. These are available, however, only for deuterium, carbon, copper and lead; we therefore used a power-law interpolation ($\sigma \propto A^\alpha$) to obtain the values shown. Our data are consistent with the results of the SLAC-E139 experiment at large x also shown in Fig. 5 which we obtained from published results [21] by dividing the ratios F_2^A/F_2^D by F_2^C/F_2^D. The errors shown for the E139 results might be overestimated since in calculating them we treated these ratios as uncorrelated. The Q^2 range covered by the E139 data is 2–11 GeV^2. No correction for a possible Q^2 dependence of the data was applied.

The ratio F_2^{Ca}/F_2^C found in the present analysis is also consistent with previous NMC results obtained from data taken at incident muon energies of 90 GeV [3] and 200 GeV [2] (see Fig. 6).

Fig. 7a shows a comparison of the present NMC data and of the ones of Refs. [2,3] with the data of the collaboration FERMILAB-E665 [26] for Ca/C and Pb/C. The NMC and E665 ratios with respect to carbon are in good agreement. Conversely, the E665 ratios with respect to the deuteron do not agree with the NMC results, as shown in Fig. 7b.

The present results combined with those of our earlier measurements of F_2^{He}/F_2^D, F_2^{Li}/F_2^D, F_2^{Ca}/F_2^D, F_2^{Ca}/F_2^C [3], and F_2^{Li}/F_2^D, F_2^C/F_2^D [2] cover the range $2 \leqslant A \leqslant 207$. From our previous measurements of F_2^A/F_2^D and F_2^C/F_2^D we calculated the ratios F_2^A/F_2^C neglecting correlations in the errors. Fig. 8 shows the structure function ratio F_2^A/F_2^C as a function of A for three selected values of x. For $A = 12$ a point at unity is included for all x bins.

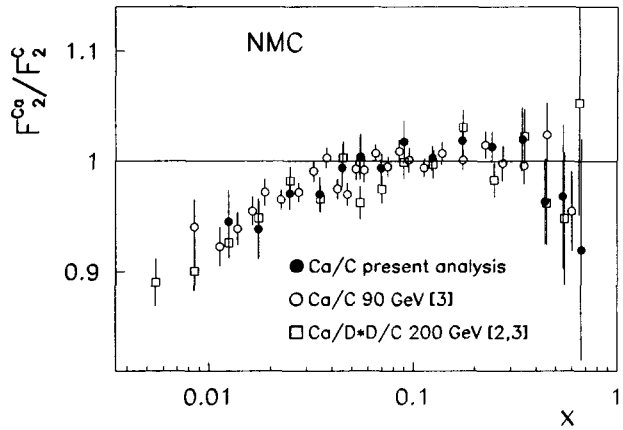

Fig. 6. The present result for F_2^{Ca}/F_2^C compared to the NMC results published in Ref. [3] (obtained at 90 GeV) and to the result obtained by dividing the F_2^{Ca}/F_2^D ratio by F_2^C/F_2^D (both obtained at 200 GeV and published in Ref. [2]). The errors were treated as uncorrelated. The error bars represent the statistical and systematic uncertainties added in quadrature. The relative normalisation uncertainty between the different data sets, not included in the error bars shown, is 0.7%.

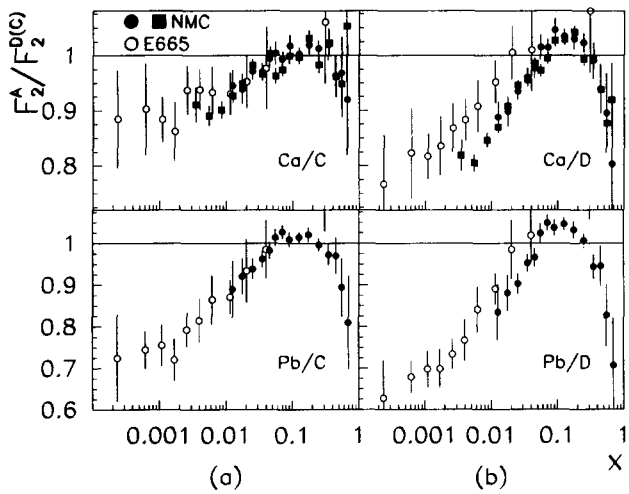

Fig. 7. Comparison of the NMC and E665 results. (a) F_2^{Ca}/F_2^C: the E665 points were obtained as (Ca/D)/(C/D), taken from Ref. [26]. The NMC points include the present results (•) and those from Ref. [2,3] already shown in Fig. 6 (□). F_2^{Pb}/F_2^C: the E665 points were obtained as (Pb/D)/(C/D), taken from Ref. [26]. The errors of the E665 results were assumed to be uncorrelated. (b) F_2^{Ca}/F_2^D: the NMC results include the present ones on Ca/C divided by the C/D data of Ref. [2] (•) and the Ca/D results of Ref. [3] (□). F_2^{Pb}/F_2^D: the NMC results (•) were obtained from the present ones on Pb/C divided by those for C/D of Ref. [2].

We parametrised the A dependence of the data in the following ways:

(i) We used the concept of the "effective number" of nucleons in the nucleus defined as $A^\alpha = \sigma_{\gamma A}/\sigma_{\gamma N}$, where $\sigma_{\gamma A}$ is the photon–nucleus cross section and $\sigma_{\gamma N}$ is the photon–nucleon cross section. Following the analysis of the E139 data, a fit to

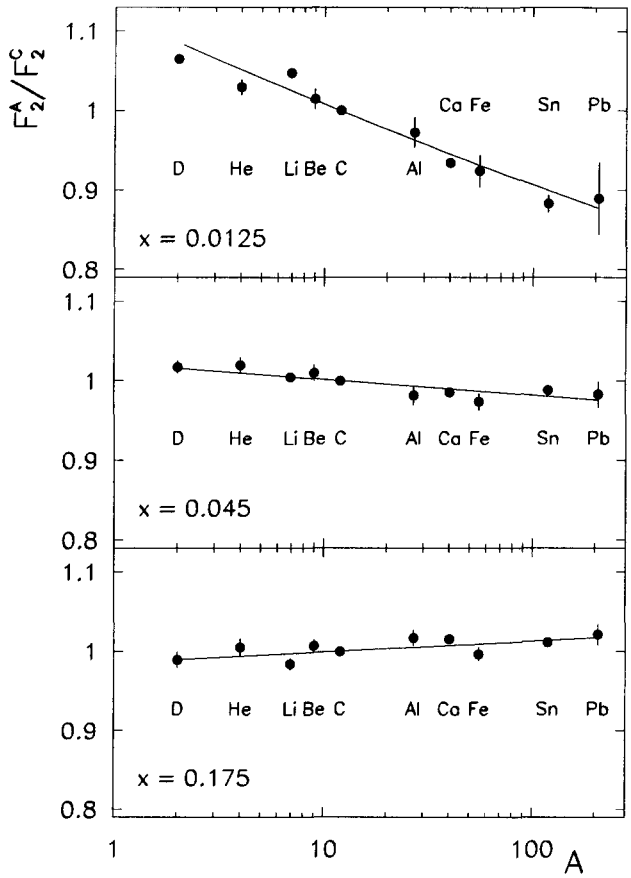

Fig. 8. Structure function ratios versus atomic weight A at $x = 0.0125$, $x = 0.045$ and $x = 0.175$. The lines show the results of fits to the data with the function $F_2^A/F_2^C = cA^{(\alpha-1)}$. The errors shown are statistical only.

the data using the function $F_2^A/F_2^C = cA^{(\alpha-1)}$ was performed in each x bin. The continuous lines in Fig. 8 show the results of the fits for three x bins. The fits describe the data satisfactorily.

(ii) The small x data are not well described by a linear function of the nuclear density, ρ, (Fig. 9): $F_2^A/F_2^C = \beta + \delta\rho(A)$, where the nuclear density is given by $\rho(A) = 3A/4\pi R_e^3$, with $R_e^2 = 5\langle r^2\rangle/3$. The mean square charge radii of the nuclei, $\langle r^2\rangle$, were taken from Ref. [17], and the assumption was made that the nuclear density distribution and the charge distributions of a nucleus are equal.

(iii) Alternatively, one can assume that the nuclear effects are due to the local properties of the nuclear medium [27]. This leads to a dependence of the nucleus cross section on a volume term (proportional to A) and a surface one (proportional to $A^{2/3}$). The structure function ratios can then be parametrised as $F_2^A/F_2^C = a + bA^{-1/3}$. The result of a fit of this function to the data is shown as solid lines in Fig. 10. The small x results are not well described. A functional form including

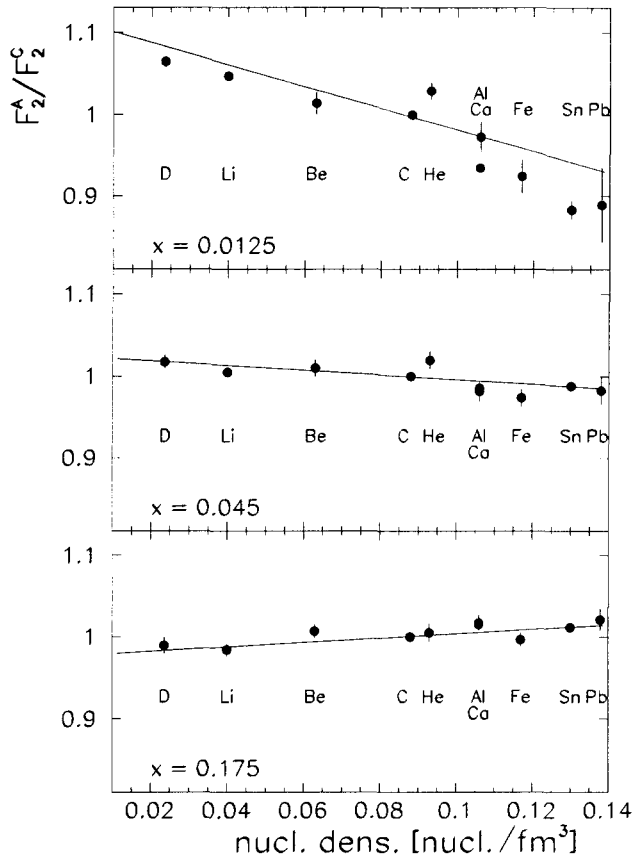

Fig. 9. Structure function ratios versus nuclear density ρ at $x = 0.0125$, $x = 0.045$ and $x = 0.175$. The solid lines show the result of a fit to the data with the function $F_2^A/F_2^C = \beta + \delta\rho(A)$. The errors shown are statistical only.

a higher order term proportional to $A^{-2/3}$ yields a significant improvement of the fit quality: the dashed line in Fig. 10 shows the result of the fit using the function $F_2^A/F_2^C = a + bA^{-1/3} + cA^{-2/3}$. Extrapolating the fitted functions to $A = \infty$ gives the nuclear matter to carbon structure function ratio, a, which is shown in Fig. 11.

(iv) A novel approach to nuclear shadowing has been recently proposed in Ref. [28], where a scaling variable n was introduced in terms of which nuclear shadowing in deep inelastic scattering is universal, i.e. independent of A, Q^2 and x. The scaling variable n is a measure of the number of gluons probed by the hadronic fluctuations of the photon. For the numerical estimates of n we used Eq. (5) of Ref. [28]. Fig. 12 shows results on structure function ratios plotted as a function of n in the range $x < 0.07$. It appears that within about 5% all the data scale with n.

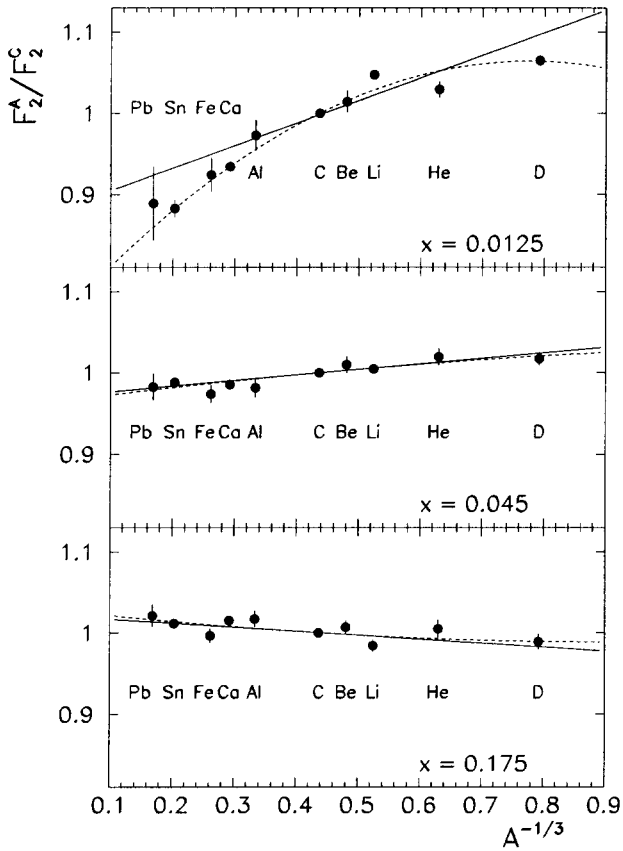

Fig. 10. Structure function ratios as a function of $A^{-1/3}$ at $x = 0.0125$, $x = 0.045$ and $x = 0.175$. The solid lines show the result of a fit to the data with the function $F_2^A/F_2^C = a + bA^{-1/3}$; the dashed lines refer to the function $F_2^A/F_2^C = a + bA^{-1/3} + cA^{-2/3}$. The errors shown are statistical only.

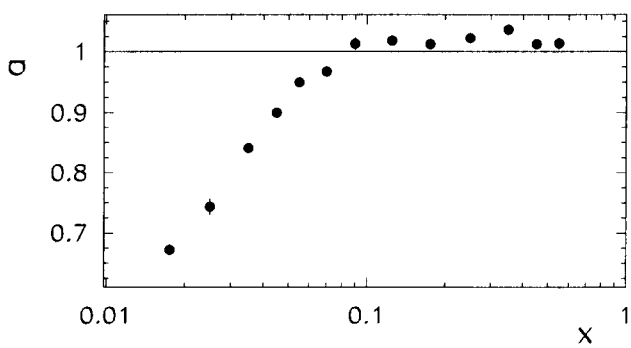

Fig. 11. The a coefficient from the fitted function $F_2^A/F_2^C = a + bA^{-1/3} + cA^{-2/3}$ is shown as a function of x.

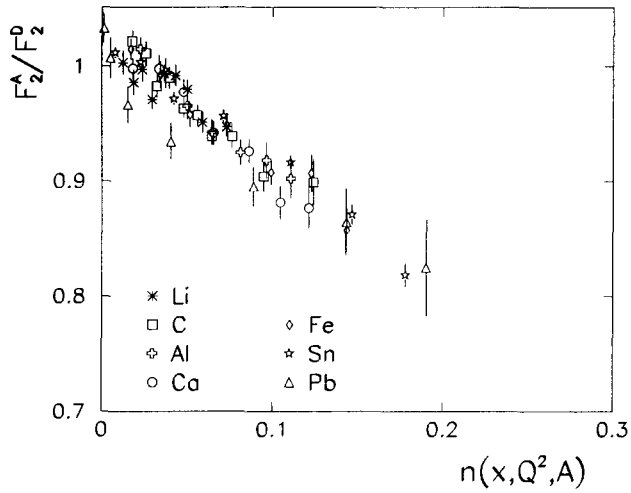

Fig. 12. Structure function ratios F_2^A/F_2^D at small x as a function of the scaling variable $n(x, Q^2, A)$. The data points include the present ones divided by the C/D data of Ref. [2] and Li/D of Ref. [3]. The errors were assumed to be uncorrelated. The errors shown are statistical only.

Acknowledgements

We thank B. Kopeliovich for kindly providing us with his program for the determination of the scaling variable n.

References

[1] For a review see, e.g., T. Sloan, G. Smadja and R. Voss, Phys. Rep. 162 (1988) 45;
L. Frankfurt and M. Strikman, Phys. Rep. 160 (1988) 235;
R.J.M. Covolan, E. Predazzi, *in* Problems of Fundamental Modern Physics, ed. R. Cherubini, P. Dalpiaz and B. Minetti (World Scientific, Singpaore, 1991) p. 85;
M. Arneodo, Phys. Rep. 240 (1994) 301.
[2] NMC, M. Arneodo et al., Nucl. Phys. B 441 (1995) 12.
[3] NMC, M. Arneodo et al., Nucl. Phys. B 441 (1995) 3.
[4] SLAC-E140, S. Dasu et al., Phys. Rev. Lett. 60 (1988) 2591.
[5] NMC, P. Amaudruz et al., Phys. Lett. B 294 (1992) 120.
[6] NMC, P. Amaudruz et al., Nucl. Phys. B 371 (1992) 3.
[7] F. Zetsche, Ph.D. thesis, Heidelberg University (1990), in German.
[8] A.A. Akhundov et al., DESY 94-115(1994); CERN-TH 7339/94 (1994); IC/94/154 (1994), to be published in Progress of Physics.
[9] K. Kurek, Z. Phys. C 63 (1994) 561.
[10] M. Gari and W. Krümpelmann, Z. Phys. A 322 (1985) 689.
[11] J. Bernabeu, Nucl. Phys. B 49 (1972) 186.
[12] E.J. Moniz, Phys. Rev. 184 (1969) 1154.
[13] A.G. Slight et al., Nucl. Phys. A 208 (1973) 157.
[14] I. Sick, Phys. Lett. B 116 (1982) 212.
[15] I. Sick et al., Phys. Lett. B 88 (1979) 245.
[16] B. Frois et al., Phys. Rev. Lett. 38 (1977) 152.
[17] H. De Vries et al., Atomic Data and Nuclear Data Tables, 36 (1987) 495.
[18] J.R. Ficenec et al., Phys. Lett. B 42 (1972) 213.

[19] L.W. Whitlow et al., Phys. Lett. B 250 (1990) 193.
[20] NMC, P. Amaudruz et al., Phys. Lett. B 295 (1992) 159.
[21] SLAC-E139, R.G. Arnold et al., Phys. Rev. Lett. 52 (1984) 727;
R.G. Arnold et al., SLAC Report SLAC-PUB-3257 (1983);
J. Gomez et al., Phys. Rev. D 49 (1994) 4348.
[22] NMC, M. Arneodo et al., Nucl. Phys. B 481 (1996) 23, next article in this issue.
[23] A. Mücklich, Ph.D thesis, Heidelberg University (1995), in German.
[24] D.O. Caldwell et al., Phys. Rev. D 7 (1973) 1362.
[25] D.O. Caldwell et al., Phys. Rev. Lett. 42 (1979) 553.
[26] FNAL-E665, M.R. Adams et al., Z. Phys. C 67 (1995) 403.
[27] I. Sick and D. Day, Phys. Lett. B 274 (1992) 16.
[28] B. Kopeliovich and B. Povh, Phys. Lett. B 367 (1996) 329. and private communications.